Particle Pusher for the Investigation of Wave-Particle Interactions in the Magnetic Centrifugal Mass Filter

Taylor Kulp-McDowall[†*], Ian Ochs[†*], Nathaniel Fisch[†*]

Princeton University[†], Princeton Plasma Physics Laboratory[*]
taylorwk@princeton.edu

September 15, 2016

Abstract

A particle pusher was constructed in MATLAB using a fourth order Runge-Kutta algorithm to investigate the wave-particle interactions within theoretical models of the Magnetic Centrifugal Mass Filter (MCMF). The model simplified to a radial electric field and a magnetic field focused in the z direction. Studies on velocity calculations were conducted in order to test the program's behavior in the large radius limit. Waves were then simulated on the rotating particles with a periodic divergenceless perturbation in the B_z component of the magnetic field. Preliminary runs indicate an agreement of the particle motion with analytical predictions—ie. cyclic contractions of the doubly rotating particle's gyroradius. Additional studies were conducted comparing the gyromotion near the resonant frequency of the pertubation and the gyromotion far from it. The resonant gyromotion was relatively constrained in comparison to the non-resonant case. It exhibited a smaller range of velocities and travelled along more defined trajectories. The orbits of the resonance case were also pushed in a specific direction by the magnetic pertubations. The next stages of the project involve the implementation of particle collisions and turbulence within the particle pusher in order to increase its accuracy and applicability to the MCMF and other rotating plasma devices.

I. Introduction and Motivation

The final goal of this project is to help further understand wave interactions of single particles within a rotating frame and apply this knowledge to the Magnetic Centrifugal Mass Filter (MCMF). This filter was proposed in Nathaniel Fisch and Abraham Fetterman's paper *The magnetic centrifugal mass filter* published in the AIP Physics of Plasma Journal in 2011. It uses both magnetic and centrifugal confinement in a similar manner to an asymmetric centrifugal trap (ACT) in order to separate light and heavy particles into different streams. The fact that these streams are outputted at opposite ends of the device in combination with the fact that the filter is collisional, allows for high throughput and large volume mass filtration. An important aspect of this filter that differentiates it both from other plasma and non-plasma filters is not only the high throughput mentioned before but also the fact that it cannot discriminate very small mass differences such as those between isotopes. This is because the filter's throughput decreases exponentially with an increase in the separation factor. Both of these characteristics makes it ideal as a practical solution for the separation of nuclear waste and nuclear fuel. It can process a lot of material at once and also provides proliferation resistance by virtue of the fact it cannot sepa-

[*]This work was supported by grant from the Princeton Environmental Institute (PEI) and the Program in Plasma Science and Technology (PPST). A great thank you goes out to both these organizations.

rate isotopes efficiently (even if it is modified)[3].

Wave particle interactions are important for the MCMF because a more general form of the alpha channeling concept described in Ian Ochs et al's *Alpha channeling with high-field launch of lower hybrid waves* and Nathaniel Fisch's *Alpha Channeling in Mirror Machines and in tokamaks* can be applied to it. In the regular tokamak case, alpha channeling describes the use of waves to incite a form of alpha particle diffusion from the fusion center to the periphery. This form of diffusion simultaneously allows for the cooling of these alpha particles via kinetic energy transfer back into the hot plasma[4]. If done correctly this technique could increase reactor efficiency by helping the fusion core maintain its temperature. The more general form of this concept was applied to rotating magnetic mirrors in Abraham Fetterman's thesis *Wave-driven rotation and mass separation in rotating magnetic mirrors*. In the context of the MCMF, the application of alpha channeling ideas aims to eliminate the need for electrodes that are typically required to drive the radial electric field and rotation. The presence of electrodes almost always limits the rotation speed of the MCMF to a velocity dubbed the Alfven velocity and thereby inhibits the filter's accuracy and efficiency. Instead of using electrodes, radio frequency waves could be used to drive rotation by creating diffusion paths in phase space for both the heavy and light ion streams[1]. Implementing this design would eliminate electrodes and be crucial to making the MCMF a viable and practical device.

The implementation of these alpha channeling wave interactions however requires knowledge of the wave-particle interactions occurring within the device, even on a single particle scale. Therefore in making the MCMF become a reality, it makes sense to study the wave-particle interactions in a rotating system that models the filter. That is exactly what this project aims to do via the construction of a particle pusher in MATLAB and the implementation of a simple MCMF model. In a broader sense the work done will not only be useful for the MCMF (although that will be the project's specific focus) but also for a wide range of ACTs and other rotating plasma devices that are being developed for fusion.

II. Particle Pusher and Initial Steps

The investigation began by the construction of a simple particle pusher within a constant magnetic and electric field. For numerical stability when solving the equations of motion, the pusher implemented a fourth order Runge-Kutta algorithm as outlined in *Low-dissipation and low-dispersion fourth-order Runge-Kutta algorithm*[5]. The code was written in MATLAB and completed near the beginning of June. The next step involved working with non-constant magnetic fields such as mirror configurations. This was finished near the middle of June. Pictures of the gyro motion for the mirror machine configuration are depicted in Figure 1 reproduced below.

III. Implementation of a Radial Electric Field

From here, the project moved toward simulating a configuration designed to replicate some of the conditions within the MCMF. A radial electric field was added with a constant magnetic field in the z direction. For simplicity during the simulation process, the code was redesigned in order to use cylindrical coordinates instead of cartesian. Figure 2 demonstrates the single particle motion within this radial configuration.

IV. Velocity Study in the Large Radius Limit

Once the code was functioning properly, the quadratic solutions to the equation of motion

Figure 1: *Particle Position over time in a mirror field configuration*

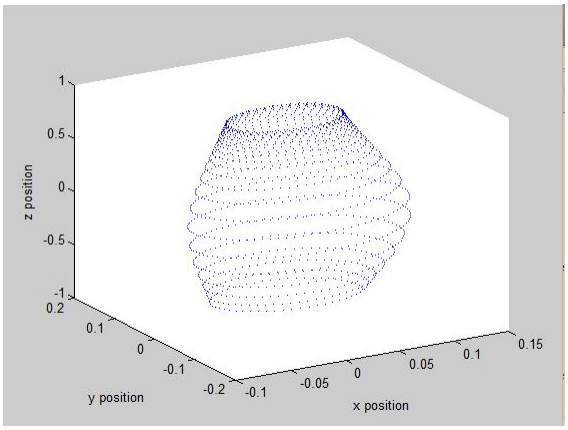

Figure 2: *Motion plot for single particle in non-perturbed magnetic field. Initial velocities were set to zero and the initial position was randomized.*

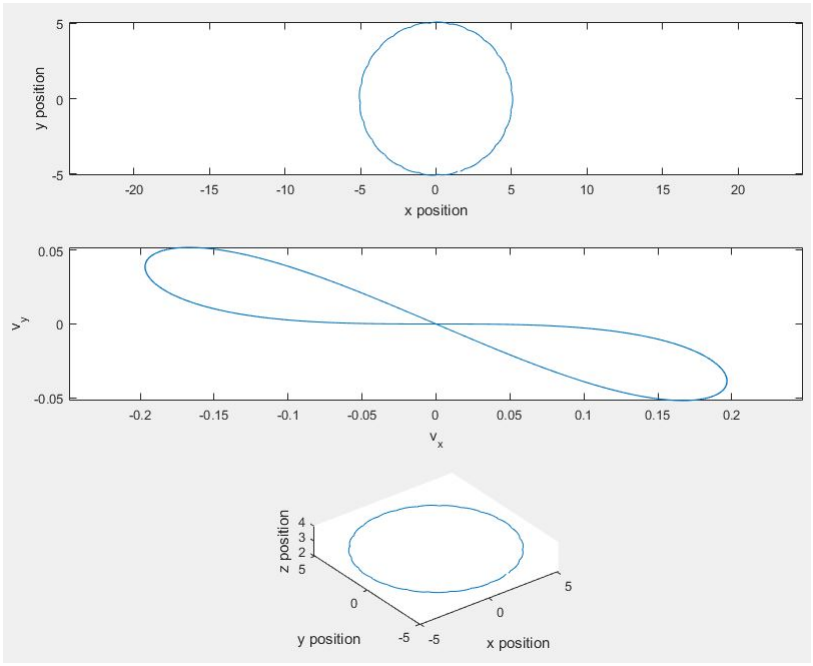

$$\frac{-mv_\theta^2}{r} = q(E + v_\theta B_z)$$

were determined to be :

$$v_\theta = \frac{rqB_z \pm \sqrt{r^2q^2B_z^2 - 4rqmE_r}}{2m}$$

Taking the two different plus and minus solutions separately we have:

$$v_- = \frac{rqB_z \pm \sqrt{r^2q^2B_z^2 - 4rqmE_r}}{2m} \quad (1)$$

$$v_+ = \frac{rqB_z \pm \sqrt{r^2q^2B_z^2 - 4rqmE_r}}{2m} \quad (2)$$

If we now expand for large r, the two solutions reduce to these approximations:

$$v_{Approx-} = \frac{E_r}{B_z} \tag{3}$$

$$v_{Approx+} = \frac{rqB_z}{m} - \frac{E_r}{B_z} \tag{4}$$

where the $v_{Approx-}$ represents the approximated large radius solution when a minus is taken in the quadratic equation and the $v_{Approx+}$ represents the large r solutions when the plus is taken. Additionally, an average velocity quantity was calculated for comparison as well. It was determined as follows:

$$v_{average} = \frac{\theta(r_{min} + \rho)}{t} \tag{5}$$

Where ρ is the gyroradius and r_{min} is the minimum radius of a complete circular orbit. These velocities were compared during the simulations in order to verify that the simulation results agreed with the analytic predictions of equations (1),(2),(3),(4), and (5) in the large radius limit.

These comparative studies were conducted using both contour plots and line graphs to see how these velocities depended on kinetic energy and average radius. The radius was varied by randomizing the r_{intial} value on each run as the average radius is directly tied to the initial r value. Analytically it was expected that there would be no dependence on kinetic energy for any of the velocities. Furthermore, a decreasing dependence on radius for v_- that plateaus at the value of $\frac{E_r}{B_z}$ was also expected. This is just asserting that the simulation should agree with the expansion for large radius done above. For the $v_{average}$ the analytical prediction was less clear as its equation does not directly depend on r but rather r_{min} and ρ which are related to r via the equations of motion. And finally for both the v_+ and the $v_{Approx+}$ velocities it was predicted that they would increase linearly with radius as both their equations are just proportional to r. For this comparison, the kinetic energy (E_k) and average radius (R) were calculated as follows:

$$E_k = \frac{q^2B^2\rho^2}{2m} \tag{6}$$

$$R = \frac{r_{max} + r_{min}}{2} \tag{7}$$

The resulting contour and line plots are reproduced in Figure 4 and Figure 3 respectively. The results in Figure 3 indicate firstly that the v_- does depend on r in the expected manner. It monotonically decreases to the $v_{Approx-}$ value at large radius. Both the v_+ and $v_{Approx+}$ values also exhibit the expected behavior. They increase linearly with radius as predicted by the analytical calculations done above. More interestingly, the $v_{average}$ behaves almost exactly as the v_- velocity. It decreases monotonically to a set value of $\frac{E_r}{B_z} = 0.2$. These results imply that the v_- velocity and the $v_{Average}$ velocity are extremely similar both in magnitude and behavior. They are also both dominated by the v_+ velocity in all cases except for extremely small radius.

On the other hand, Figure 4 depicts some worrying results. There is some sort of weird kinetic energy dependence that disagrees with analytical predictions and has no consistent physical explanation. The cause of this inconsistency will be discussed in the next section.

V. Problematic Kinetic Energy Dependence

During the velocity study conducted above it was noticed that both the minus and average velocity exhibited a problematic form of kinetic energy dependence. This problematic behavior was seen through the construction of contour plots that showed the dependence of velocities on radius and kinetic energy. Some of these are shown in Figure 4. The results exhibit the decrease in v_- and $v_{average}$ as r increases consistent with Figure 3 however also includes a kinetic energy dependence conditional on radius. This was problematic because even when the simulation was initialized with zero kinetic energy fluctuations/dependence still persisted. Additionally, both v_- and $v_{average}$ do not depend explicitly on any of the variables that E_k does (other than the magnetic field which is

Figure 3: *Velocity comparison plots. In this configuration $E_r = 1$ and $B_z = 5$. The last graph depicts both average velocity and minus velocity on the same plot. They both overlap almost exactly.*

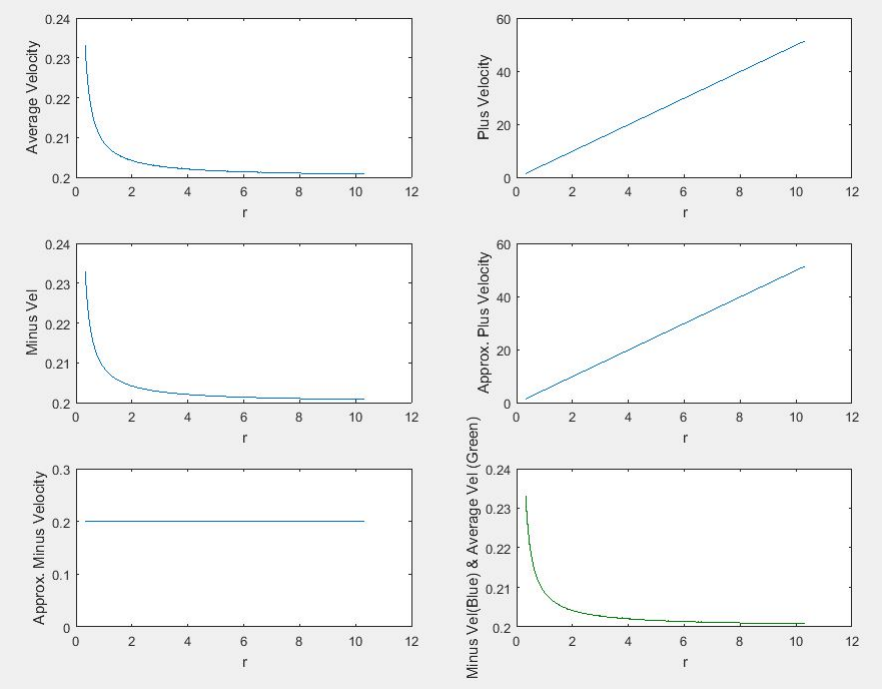

constant) and so something is definitely going wrong. One possible non-physical explanation for this problem is related to a numerical error in the calculation of the average radius and gyroradius at small values. It is also important to note that the r used for calculating all of the different velocities was in fact the average radius (R) as it best models the radius of the orbital gyromotion as a whole. The gyroradius and average radius calculations are indirectly related, namely by the minimum and maximum calculations shown below.

$$\rho = \frac{r_{max} - r_{min}}{2}$$

$$R = \frac{r_{max} + r_{min}}{2}$$

So it is possible that if the minimum and maximum calculations (or their sum or difference for that matter) produced a numerical error for small values of the cylindrical coordinate r both ρ and R would both become related in some intertwined yet unpredictable way. Consequently, an erratic relationship between the velocities and kinetic energy would be seen for small values of E_k and the expected lack of relationship would be seen for bigger values. In order to see whether this was the case, both the velocities' dependence only on kinetic energy were graphed. The results are depicted in Figure 5.

The random and scattered behavior in this graph is evidence that the error did indeed arise from numeric instability within the simulation. More evidence of this is that the erratic behavior only occurs for small values of kinetic energy and then completely dies off at kinetic energies above 0.001. Because the behavior instantly nullify after a kinetic energy of 0.01 it can be safely ignored anywhere above this range. The work done in this paper safely satisfies this condition as the initial velocity is never initialized to be $-v_\theta$ and always set to give kinetic energies above such a small value. This is assured in practice by adding a small initial value of $\frac{8}{25}$ to the $r_{initial}$, $\theta_{initial}$,

Figure 4: *The problematic kinetic energy dependence. This contour depicts the dependence of the average velocity, the v_- , the v_+ velocity, and the approximate v_+ velocity on the average radius (R) and the kinetic energy E_k. The contour should only show vertical patterns as there should be no kinetic energy dependence for both the $v_{average}$ and v_-. In this configuration $E_r = 1$ and $B_z = 5$ and the initial $v_\theta = -v_-$.*

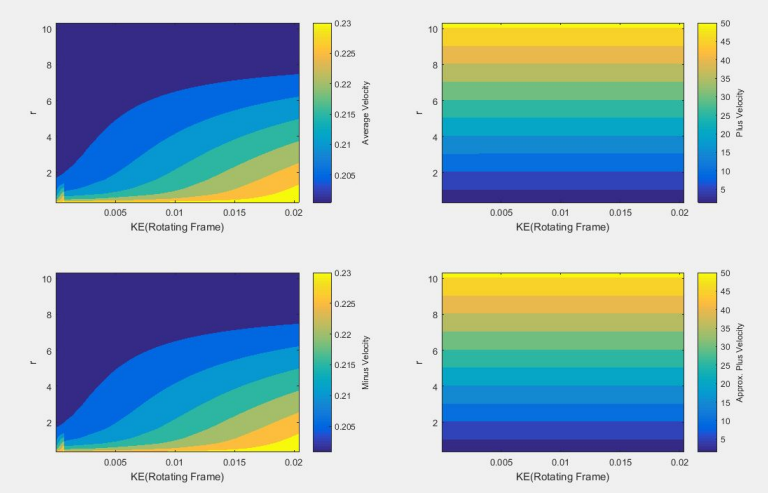

and $z_{initial}$ that always keeps the kinetic energy above such small values. This value was determined through running the simulation for various small initial conditions and noting the value above which the problematic kinetic energy dependence disappeared.

VI. Addition of Perturbations

Perturbations were then added to the magnetic field in order to represent waves effects in the rotating frame. The wave effects in a realistic scenario would be a result of the alpha channeling phenomena introduced in the first motivation paragraph. A periodic divergence-less magnetic perpetuation was added to the B_z component of the magnetic field. The magnetic field evolved according to:

$$\vec{B_z} = B_{initial} + b|\sin(n|\theta|)| \tag{8}$$

The b out front is a small constant included in order to make the perturbation on a realistic scale in relation to the magnetic field. The absolute value on the sine function perturbation was included in order to make the perturbations never negative and only exist within the range [0,1]. This was needed to eliminate the possibility that the perturbation would lower the magnetic field enough to bring the kinetic energy into the range where the numerical errors described above would occur. Other solutions to this issue that would not involve using absolute values will be explored in future work. In terms of the parameters, $B_{initial}$ was set to 5. Both the B_r and B_θ components of the magnetic field were set to zero. The n was initially set to 9 which was calculated to represent a non-resonant wave frequency that will be useful for the next section. The n value will be changed later when the frequency of the perturbation needs to be specified namely in the case of resonance. The b value was set to 0.5. Reproduced in Figure 6 are some plots of the single particle motion within the perturbed fields with $n = 9$. Notice that the gyromotion on the circular perimeter is not only out of "phase" on the second and third circular orbits but also reaches slightly different maximum radi. If one zooms in close enough as well it can be seen that the small loops at turning points for near r_{min} motion are not all the same. Namely some of the orbits have consistently bigger reversal loops than the others.

Figure 5: *The kinetic energy dependence of the velocities is erratic and scattered at the beginning becoming null later on. In this configuration $E_r = 1$ and $B_z = 5$.*

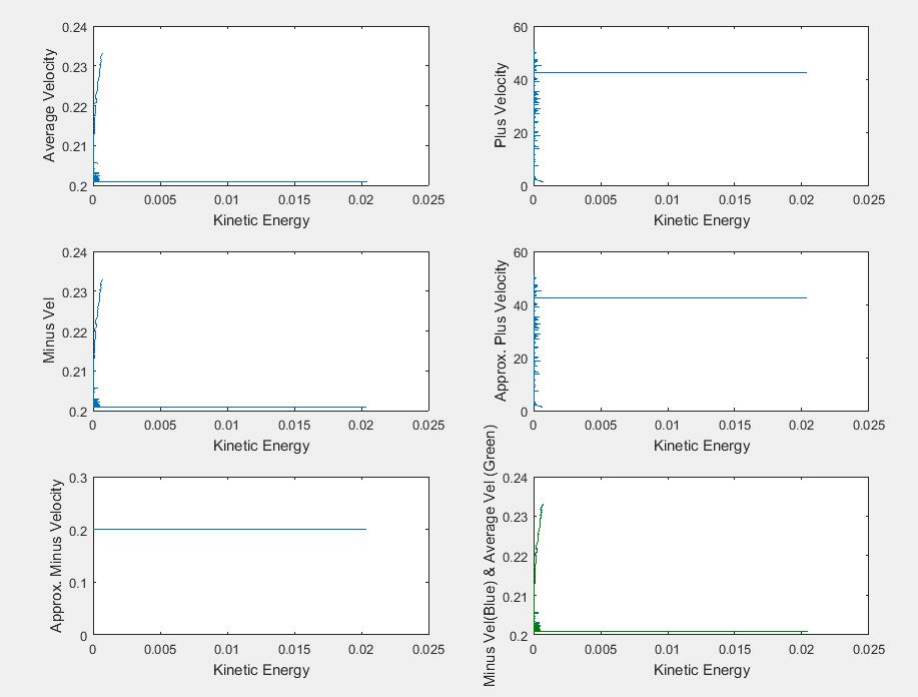

VII. Resonance and Perturbations Investigation

The next step involved a comparative study of the resonant versus non-resonant behavior of the perturbed system. In order to achieve ion cyclotron resonance, the plasma angular frequency $\omega_p = \frac{qB}{m}$ was approximately matched to the resonant frequency which required the condition:

$$\frac{m}{q} = \frac{B}{2\pi f_p}$$

where m,q,B, and f_p are the mass, charge, magnetic field, and frequency of perturbation respectively. This means that the condition for resonance is that the frequency of the magnetic field perturbation is:

$$f_p = \frac{Bq}{2\pi m}$$

The frequency f_p is used here and not the angular frequency ω_p because it is slightly easier to match the frequency of the perturbation when varying f_p. For this study the values used were: $m = 1$, $B = 5$, $q = 1$ and so the frequency desired for resonance was:

$$f_p = \frac{5}{2\pi}$$

This frequency was achieved by altering the form of the perturbation. The form that gave an approximate (to 4 decimal places) frequency of $\frac{5}{2\pi}$ was:

$$\vec{B_z} = 5 + 0.5|\sin(46.599|\theta|)|$$

The motion graphs for resonance and near-resonance were then produced and compared to the motion plots for non-resonant systems. The results of this study are depicted in Figure 6 for the non-resonant case and Figure 7 for the resonant case.

As depicted there is a noticeable difference between the the non-resonant and resonant cases. The difference is initially seen in the velocity plot. The non-resonant case exhibits

Figure 6: *Close up on the motion plot for single particle in perturbed magnetic field in order to demonstrate the out of phase oscillations. The n value was set to 9 to give non-resonant behavior. Initial velocities were set to zero and the initial r position was set to 1 while the initial theta and z were both zero. The red dot represents the initial starting position. The full image of the motion was a circle that extended upon the oscillations pattern depicted in the image.*

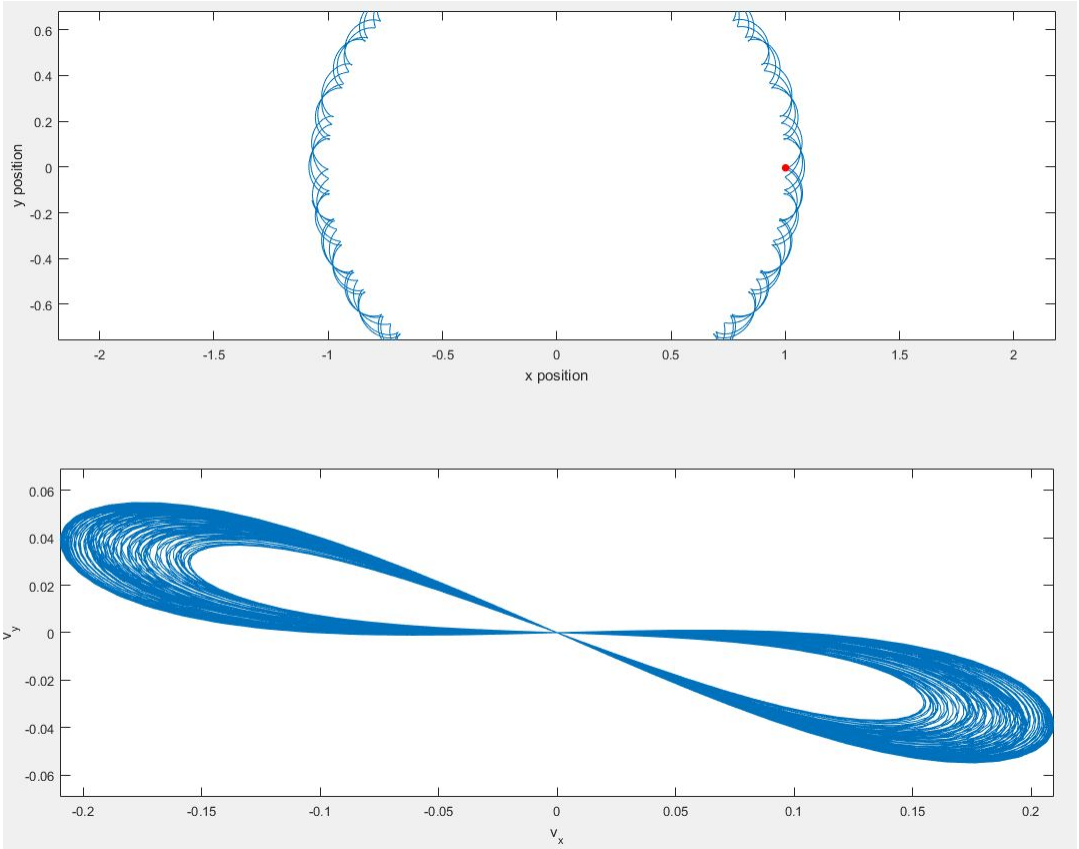

a broader range of velocities shown by the greater thickness of the "infinity band" especially toward the upper left and lower right edges. In comparison, the velocity of the resonance case is more constrained having an all around thinner "infinity band". This fact is related to the general observation that the resonant gyromotion followed a more definite trajectory when compared to that of the non-resonant case. The velocities do not vary as much between orbits in the resonant case implying that each successive trajectory is closer to the previous one than in the non-resonant case. Additionally, one can notice that in the resonant case after each successive orbit the orbital gyromotion of the particle is shifted downward by a constant amount. This means that the resonant wave is pushing the orbital gyromotion of the particle uniformly in a certain direction. In this case that direction is the negative y direction. If one now views the non-resonant case in the same light the orbital gyromotion seems more to be "shaken up" then directed. This is intuitive because no resonance implies the lack of in-phase interactions between the magnetic field perturbations and the motion of the particle. The magnetic field perturbation will not be in sync with the particle motion and so it will never push in only one specific direction which is the requirement for directing the orbital gyromotion.

Figure 7: *Close up on the motion plot for single particle in perturbed magnetic field. The n value was set to the calculated 46.599 to make the system exhibit resonant behavior. Initial velocities were set to zero and the initial position was set to the same as that in Figure 6 to make comparison easier. The red dot represents the initial starting position. The full image of the motion was a circle with the same continuous oscillations pattern depicted in the image.*

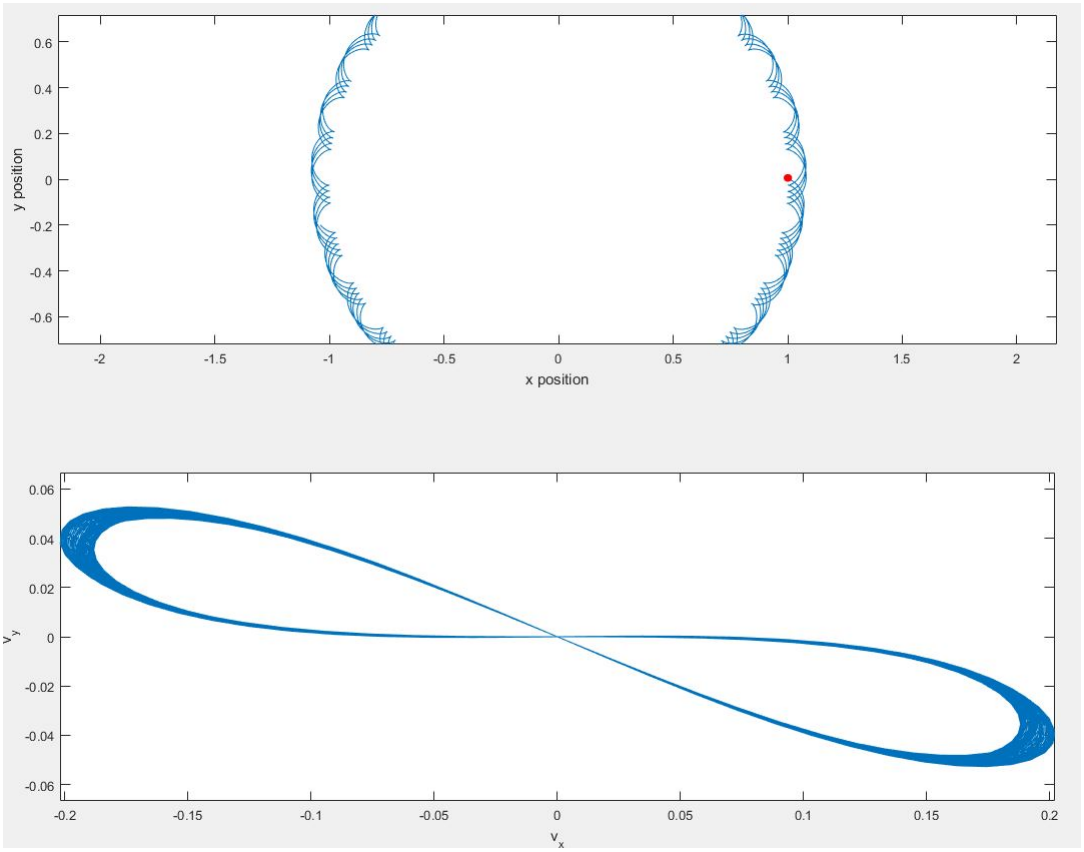

Future Directions

This project is still in development and will continue over the next year. Further work will be conducted on the resonance studies described above more specifically on different types of perturbations such as the removing the absolute value signs. Studies will also be conducted on the oscillations modes of the gyroradius for various perturbations including the current one. This will give insight into the resonance and non-resonance behavior of the gyroradius. For the long term, there are many directions in which this project can take. One of the most probable is the implementation of multiple particles, their interactions, and the resulting plasma turbulence. With these new features, larger scale simulations would be possible and new dynamic processes would arise specifically in the rotating frame of reference. This would provide a large amount of interesting behavior to study. This would also make the model much more suited to modeling the MCMF on a larger scale which would have practical diagnostic and predictive benefits.

References

[**1.** Abraham J. Fetterman, 2012] Wave-driven rotation and mass separation in rotating magnetic mirrors study; *Thesis submitted to Princeton University*

[**2.** I. E. Ochs, N. Bertelli, and N. J. Fisch, 2015] Alpha channeling with high-field launch of lower hybrid waves; *Phys. Plasmas 22, 112103 (2015)*

[**3.** Abraham J. Fetterman, Nathaniel J. Fisch 2012] The magnetic centrifugal mass filter; *Phys. Plasmas 18, 094503 (2011)*

[**4.** Nathaniel J. Fisch 2007] Alpha Channeling in Mirror Machines and in tokamaks; *Fusion Science and Technology Volume 51 Number 2T February 2007 Pages 1-6*

[**5.** Julien Berland Christophe Bogey Christophe Bailly 2006] Low-dissipation and low-dispersion fourth-order Runge-Kutta algorithm; *Computers & Fluids Volume 35 Issue 10 December 2006 Pages 1459-1463*

VIII. Acknowledgments

I would like to thank Professor Nat Fisch for both helping me set up the project and supporting me throughout the research process. Furthermore, I am especially grateful to Ian Ochs for constantly meeting with me on a moments notice and always helping to guide me along the research path. Additionally, this work could have not been done without the help of Professor Samuel Cohen who met with me in person to introduce me to the PPST Internship program and facilitated my assignment. Thank you also to the Princeton Environment Institute (PEI) and the Program in Plasma Science and Technology (PPST) for the constant support during the summer.